Biochimica et Biophysica Acta 1807 (2011) 769–778

Contents lists available at ScienceDirect

Biochimica et Biophysica Acta

journal homepage: www.elsevier.com/locate/bbabio

A combined quantum chemical and crystallographic study on the oxidized binuclear center of cytochrome *c* oxidase

Ville R.I. Kaila [a,b,*], Esko Oksanen [c,1], Adrian Goldman [c], Dmitry A. Bloch [a], Michael I. Verkhovsky [a], Dage Sundholm [b], Mårten Wikström [a]

[a] Helsinki Bioenergetics Group, Structural Biology and Biophysics Programme, Institute of Biotechnology, University of Helsinki, P. O. Box 65, FI-00014 Helsinki, Finland
[b] Department of Chemistry, P. O. Box 55 (A.I. Virtanens plats 1), FI-00014 University of Helsinki, Helsinki, Finland
[c] Macromolecular Structures Group, Structural Biology and Biophysics Programme, Institute of Biotechnology, University of Helsinki, P. O. Box 65, FI-00014 Helsinki, Finland

ARTICLE INFO

Article history:
Received 15 April 2010
Received in revised form 20 December 2010
Accepted 26 December 2010
Available online 4 January 2011

Keywords:
Heme-copper oxidases
Oxygen binding
Density functional theory (DFT)
X-ray refinement

ABSTRACT

Cytochrome *c* oxidase (C*c*O) is the terminal enzyme of the respiratory chain. By reducing oxygen to water, it generates a proton gradient across the mitochondrial or bacterial membrane. Recently, two independent X-ray crystallographic studies ((Aoyama et al. Proc. Natl. Acad. Sci. USA 106 (2009) 2165–2169) and (Koepke et al. Biochim. Biophys. Acta 1787 (2009) 635–645)), suggested that a peroxide dianion might be bound to the active site of oxidized C*c*O. We have investigated this hypothesis by combining quantum chemical calculations with a re-refinement of the X-ray crystallographic data and optical spectroscopic measurements. Our data suggest that dianionic peroxide, superoxide, and dioxygen all form a similar superoxide species when inserted into a fully oxidized ferric/cupric binuclear site (BNC). We argue that stable peroxides are unlikely to be confined within the oxidized BNC since that would be expected to lead to bond splitting and formation of the catalytic P intermediate. Somewhat surprisingly, we find that binding of dioxygen to the oxidized binuclear site is weakly exergonic, and hence, the observed structure might have resulted from dioxygen itself or from superoxide generated from O_2 by the X-ray beam. We show that the presence of O_2 is consistent with the X-ray data. We also discuss how other structures, such as a mixture of the aqueous species ($H_2O + OH^-$ and H_2O) and chloride fit the experimental data.

1. Introduction

Cytochrome *c* oxidase (C*c*O) is responsible for more than 90% of biological oxygen consumption on Earth [1]. Coupled to oxygen reduction to water, it contributes to creating an electrochemical proton gradient across the mitochondrial inner membrane, which is used for synthesis of ATP by F_oF_1-ATPase and for active transport [2–4]. Oxygen reduction to water as catalyzed by C*c*O does not release harmful oxygenous compounds in the cell [5]. These compounds, commonly known as reactive oxygen species (ROS), are formed upon incomplete reduction of oxygen (or oxidation of water). Full reduction of oxygen to water requires four electrons, while partial two electron reduction produces (hydrogen) peroxide (Fig. 1A). Superoxide ($O_2^{*/-}$) and hydroxyl radicals (OH^*) are formed by one electron reduction of oxygen and peroxide, respectively. These are the major ROS compounds of which particularly the latter is very harmful for the organism due to its high reactivity. Accumulation of ROS has been shown to lead to many pathological conditions [6].

The active site of C*c*O comprises two metal ions—a high-spin heme, heme a_3, and a copper ion, Cu_B (see Fig. 1B). Cu_B is ligated to three histidines (His-240, His-290, His-291), one of which (His-240) is covalently linked by its side chain to a tyrosine residue (Tyr-244), which modifies the proton and electron affinities of the tyrosine [7–10]. The reaction cycle of C*c*O begins by binding molecular oxygen to the fully reduced binuclear center (BNC) in state R. The formed species, known as state A [11] (see Fig. 1C), has an open-shell singlet configuration and is best described as a ferric superoxide species [12,13]. After formation of the oxygen adduct, the dioxygen bond is split in one step. In the O_2-splitting reaction, four electrons are taken from the binuclear site: two from heme a_3, one from the copper of Cu_B, and the fourth most probably from the covalently linked Tyr-244 together with its phenolic proton [1,14,15]. The reaction leads to formation of a ferryl heme ($Fe[IV] = O^{2-}$), a cupric Cu_B ($Cu[II]\text{-}OH^-$), and a neutral tyrosine radical ($Tyr\text{-}O^*$)—a state known as P_M because it was originally thought to be a ferric/cupric peroxide compound. This first reaction step transfers the oxidative power of O_2 to the enzyme active site and produces two oxygenous species (the ferryl oxo and the cupric hydroxo) at the redox level of

* Corresponding author. Laboratory of Chemical Physics, National Institute of Diabetes and Digestive and Kidney Diseases, National Institutes of Health, Bethesda, Maryland 20892-0520, USA. Tel.: +1 3014515984; fax: +1 301 496 0825.
E-mail address: ville.kaila@nih.gov (V.R.I. Kaila).
[1] Present address: Institut de Biologie Structurale (UMR 5075 CEA-CNRS-UJF), 46 rue Jules Horowitz, 38027 Grenoble Cedex 1, France.

0005-2728/$ – see front matter © 2011 Elsevier B.V. All rights reserved.
doi:10.1016/j.bbabio.2010.12.016

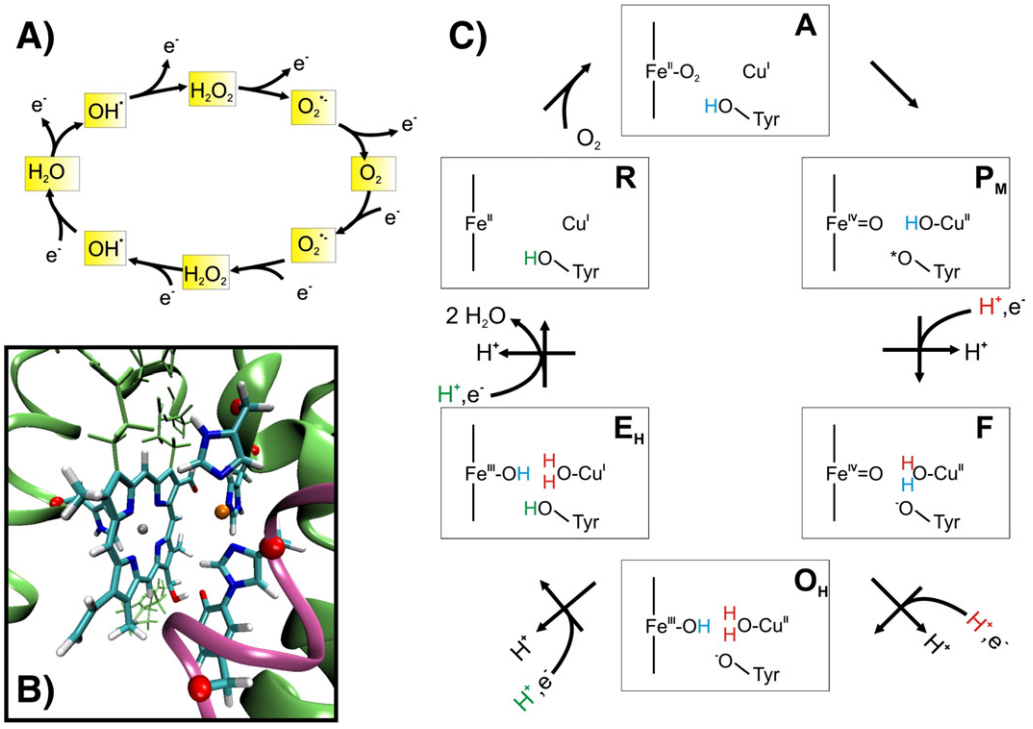

Fig. 1. A) Different oxidation states of oxygen: superoxide ($O_2^{*/-}$), hydrogen peroxide (H_2O_2), hydroxyl radical (OH^*), and water. B) The structure of the binuclear center (BNC) of cytochrome *c* oxidase. In addition to heme a_3 and the copper of Cu_B, the figure shows His-376, His-240, Tyr-244, His-290, and His-291. C) The catalytic cycle of cytochrome *c* oxidase (see text). Protons taken from the D-channel and K-channel are shown in red and green, respectively.

water. In the remaining steps of the reaction cycle, the oxo and hydroxo species are stepwise protonated and the electrons are replenished by the electron donor, cytochrome *c*. The P_M state can be produced artificially from the fully oxidized O state (see below) by letting C*c*O react with hydrogen peroxide [16,17]. Hydrogen peroxide can be thought of as oxygen with two additional protons and electrons (Fig. 1A), which are required to convert the O state to the reduced R state, which then further reacts with oxygen to produce P_M [18]. However, intermediates in this artificial hydrogen peroxide reaction have not been observed, which suggests that P_M is produced concertedly from O or, alternatively, that the reaction intermediates are very short lived.

The oxidized binuclear site (O state) is characterized by ferric heme a_3 (Fe[III]) and cupric Cu_B (Cu[II]), which can be identified spectroscopically by the specific position of the optical absorbance bands and the presence of a heme charge transfer band [19]. In the O state, Tyr-244 has been reported to have a pK_a of 6.5 [20], and the ligands of the BNC metals have usually been thought to be water and hydroxide. Phenomenologically, the oxidized state of the binuclear center occurs in two different forms: the O_H state, which is linked to proton-pumping and occupied during steady state turnover, and the O state, which is found in the enzyme as isolated [21–23]. Unfortunately, the two states have identical spectroscopic signatures [19], and it has been suggested that the O state might represent a dehydrated form of the active site [24].

Early crystal structures of oxidized C*c*O showed continuous electron density between the heme iron and Cu_B, usually interpreted as an aquo and an OH^- ligand (see above). However, more recently with higher resolution X-ray data, two research groups have interpreted this density quite differently. Aoyama et al. [25] suggested that a peroxide dianion (O_2^{2-}) bridges between the metals of the oxidized binuclear site, a conclusion that was mainly reached based on an O–O distance of 1.7 Å. Since the shortest observed O–O distance of hydrogen-bonded structures found in inorganic bimetallic centers is 2.5 Å, the oxygen atoms must be connected by a covalent bond, excluding hydrogen-bonded structures. It was further suggested that the peroxide might be an inhibitor and a possible molecular explanation for the non-pumping O state. Based on similar arguments, Koepke et al. [26] also concluded that the electron density is well described by a peroxide dianion. Both groups excluded a chloride anion that would otherwise be a fair candidate, based on tests with bromide [26] and use of chloride-free media [25].

In this work, we present quantum chemical density functional theory (DFT) calculations on a structural model and their consistency with the X-ray data. This allows us to evaluate the likelihood of different oxygenous compounds in the oxidized binuclear site of C*c*O. Together, these approaches give insight in the molecular nature of the oxygenous species found in the recent crystallographic studies.

2. Models and methods

2.1. DFT calculations

Model systems of the binuclear site were constructed based on the X-ray structure of oxidized C*c*O from *Bos taurus*, PDB entry 2ZXW [25]. The model comprised ~140 atoms including heme a_3 without its propionate groups, the copper atom of Cu_B, and residues His-376, His-240, His-290, His-291, and Tyr-244. The amino acids were terminated at the alpha carbons, which were fixed to their crystallographic position during structure optimization. The structure of the oxidized binuclear site was optimized in 30 different ligand states using the BP86 functional [27,28], due to its good performance on geometries [29], and the multipole accelerated resolution of identity approximation (MARIJ-RI) [30]. All atoms were described by a def2-SVP basis set [31] except for the metals which were described by a larger def2-TZVP basis set [32]. After structure optimization, single point calculations were performed using the B3LYP functional [33,34] due to its better performance on energetics as compared to the BP86 functional [29,35–37] using def2-TZVP basis set on all atoms. Siegbahn et al. [38] have recently suggested that dispersive interactions are important for

binding small molecules to metal centers. Dispersive effects were studied by the empirical dispersion correction by Grimme [39,40]. Solvation effects were studied by the COSMO model [41] using a dielectric constant set to 4. In the oxidized binuclear site models, heme a_3 iron was modeled in the high-spin ferric state anti-ferromagnetically coupled to cupric copper, in accordance with extensive work by Siegbahn et al. [42]. Different spin states have been found to reside close in energy, and DFT is not considered sufficiently accurate to discriminate the energetical ordering of the state [43,44]. The oxy-ferrous/cuprous model was modeled as an open-shell singlet state. A smaller model, comprising only heme a_3, was also studied by the same methodology described above. All calculations were performed with TURBOMOLE v. 5.9 and 6.0 [45].

2.2. Crystallographic re-refinement

The structure factors and a model of oxidized CcO from *B. taurus* (entry 2ZXW [25]) were obtained from the Brookhaven Protein Databank. The coordinates include some non-protein atoms with B-factors over 100 Å^2. For unbiased refinement, non-protein atoms were removed from the model. After refinement in REFMAC5 [46], the metals, water, and detergent molecules that were clearly visible in the maximum likelihood weighted maps [47] (electron density above 1 σ) were modeled with Coot [48] with their B-factors set to 20 Å^2 and the structure re-refined. In the process, we also had to remodel the C-termini of chains Q and Z; our final B-factors are slightly lower than in the original structure.

The coordinates from the DFT calculations were superposed on the metals and their ligating nitrogen atoms using pairwise alignment in PyMOL [49]. The reason for this was that the resolution of the data and the restraint model available to us does not allow deviations from planarity of the porphyrin ring to be modeled properly. Therefore, an all-atom fit to the DFT optimized structures tends not to superpose the metal ions. We tested various superposition methods and found that using the metals and their eight ligating nitrogen atoms (porphyrin and histidine nitrogens) gave the most meaningful superpositions. This choice is also justified by the fact that the metal positions are much more precisely defined in the crystal structure than the lighter atoms. The coordinates of the species between the metal ions were then replaced by those obtained from the DFT calculations. After further refinement in REFMAC5 to avoid unrealistic bond lengths, electron density maps were calculated with FFT in the CCP4 package [50]. The R_{work}/R_{free} was 0.211/0.246 for the model with O_2. The R-factors were slightly higher than in the original structure (Table 1), but the difference between R_{work} and R_{free} was smaller.

2.3. Optical measurements

Optical measurements of CcO from *Rhodobacter sphaeroides* and *B. taurus* were performed at pH 6.5 in 100 mM MES-buffer with 0.15 % dodecylmaltoside, in the presence of 0.3 mM ferricyanide under anaerobic conditions. The UV–VIS spectra were measured for each intermediate step during 15 cycles of degassing, after which oxygen was added to the sample.

Table 1
The R-factors for the models with different active site contents.

Active site content	R_{work}	R_{free}
$O_2/O_2^*/-/O_2^{2-}$	0.211	0.246
H_2O/OH^-	0.210	0.230
50% H_2O on each metal	0.211	0.245
50% one H_2O + 50 % H_2O/OH^-	0.215	0.235
Cl^-	0.211	0.245
2ZXW [25]	0.185	0.233
3HB3 [26]	0.220	0.280

3. Results and discussion

3.1. Comparison of DFT and X-ray structures

Comparing and combining information from X-ray crystallography and QM calculations are challenging tasks [51]. An X-ray structure is usually presented as atomic coordinates and displacement factors, but it has to be kept in mind that these coordinates are just a model used to interpret the electron density map. The situation is further complicated by model bias; the map itself is biased by the iterative structure refinement. The correctness of the structure is often assessed by global indicators such as the crystallographic residual (R-value) and the statistically independent residual R_{free} [52]. These numbers measure the difference between the observed structure factors and those calculated from the coordinates. The absolute value of either R or R_{free} depends on how the structure factors are calculated from the model, and the model depends on the refinement software used—and in any case they are very insensitive to changes in just a small part of the structure. The differences between the models presented here are small enough not to make a significant difference in R or R_{free}, so the consistency with the data has to be assessed in real space by the electron density maps. This is indeed the standard way of interpreting small changes in the active sites of proteins and is perforce subjective. Numerical indicators such as the real space R [53] can detect serious errors in map interpretation but cannot distinguish between models that differ only slightly. The models presented below do not differ drastically in their fit to the electron density maps, so from a crystallographic point of view, they are all plausible models. The DFT calculations along with subtle differences in the fit suggest that molecular oxygen is the most reasonable species to occupy the binuclear site.

Table 2
Optimum geometries for different species bound to the oxidized binuclear site. All distances are given in angstrom.

Ligand	Tyr-244	O–O	Fe–O	Fe–His	Cu–O	Fe–Cu
O_2^{2-}	YOH	1.30	2.23	2.28	2.02	4.85
O_2^{2-}	YO^-	1.31	2.17	2.31	2.02	4.77
HOO^-	YOH	1.41	2.11	2.26	2.22	4.93
HOO^-	YO^-	1.44	2.01	2.32	2.20	4.90
HOOH	YOH	1.46	2.72	2.13	2.40	5.60
HOOH	YO^-	1.47	2.54	2.15	2.45	5.57
O_2	YOH	1.29	1.91	2.01	2.16	4.79
O_2	YO^-	1.29	1.87	2.01	2.08	4.66
$O_2^*/-$	YOH	1.32	1.89	2.02	2.02	4.59
$O_2^*/-$	YO^-	1.32	1.85	2.02	2.03	4.57
$H_2O/-$	YOH	1.98[a]	2.50	2.15	4.55	6.44
$-/H_2O$	YOH	1.98[a]	3.58	2.10	2.24	5.59
$H_2O/-$	YO^-	1.47[b]	2.46	2.16	3.90	5.85
$-/H_2O$	YO^-	1.47[b]	3.37	2.11	2.33	5.51
H_2O/OH^-	YOH	2.53	2.21	2.22	1.94	5.36
H_2O/OH^-	YO^-	2.47	2.02	2.31	2.13	5.29
OH^-/OH^-	YOH	2.75	1.90	2.49	1.92	4.71
OH^-/OH^-	YO^-	2.65	1.93	2.55	1.96	4.19
O^{2-}/OH^-	YOH	2.69	1.66	2.11	1.89	4.90
O^{2-}/OH^-	YO^-	2.62	1.96	2.62	1.87	4.11
$-/-$	YOH	–	–	2.11	–	5.12
$-/-$	YO^-	–	–	2.12	–	5.74
Cl^-	YOH	–	3.34[c]	2.15	2.29[c]	5.12
Cl^-	YO^-	–	2.55[c]	2.27	2.41[c]	4.58
Br^-	YOH	–	3.46[c]	2.15	2.43[c]	5.18
Br^-	YO^-	–	2.81[c]	2.24	2.48[c]	4.66
Fe[II]/O_2/Cu[I]	YOH	1.32	1.80	2.05	2.02	4.10
X-ray [2ZXW]	–	1.70	2.23	2.08	2.08	4.88
X-ray [3HB3]	–	1.49	1.93	1.94	1.92	4.62

[a] The O–O distance is calculated from superimposed $H_2O/-$ and $-/H_2O$ structures with Tyr-244 protonated.
[b] The O–O distance is calculated from superimposed $H_2O/-$ and $-/H_2O$ with Tyr-244 deprotonated.
[c] Halogen-metal distance.

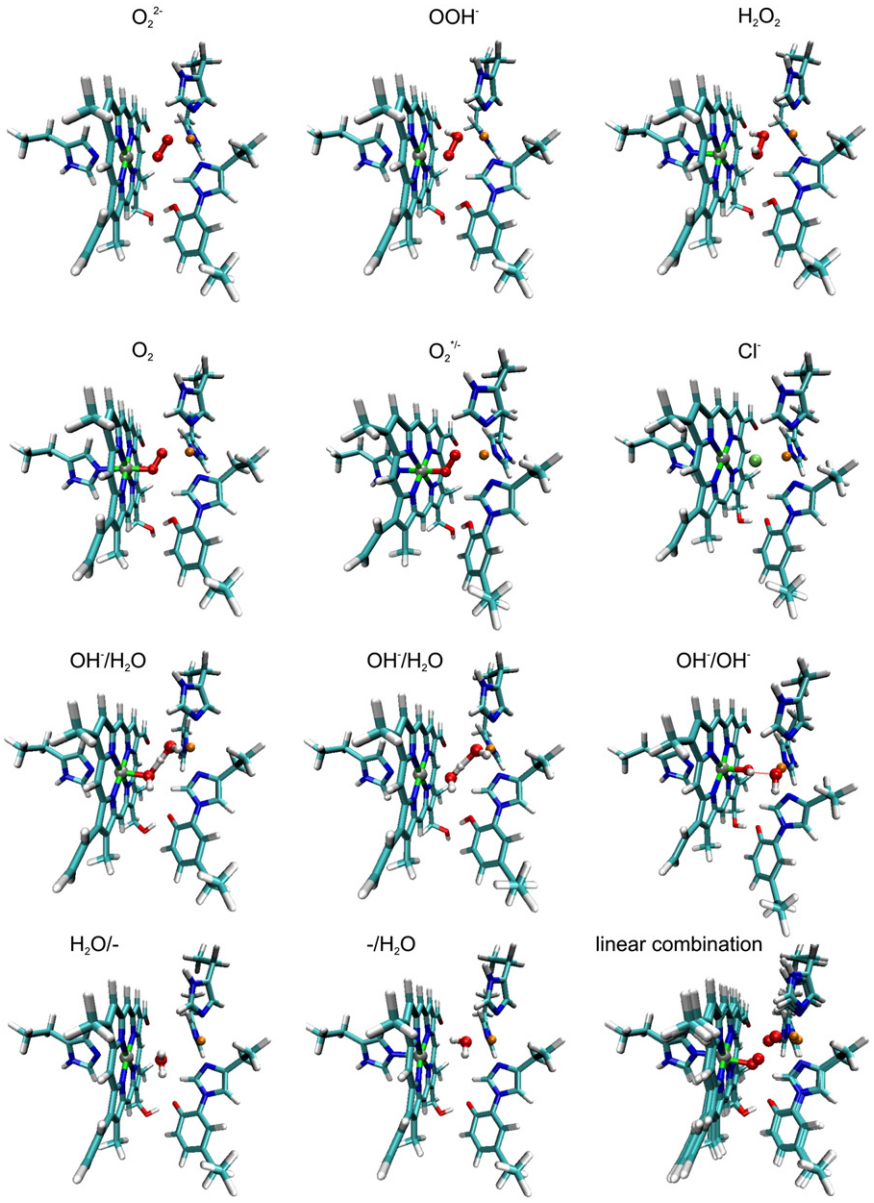

Fig. 2. Geometries of some selected structures. First row: peroxides in different protonation states; second row (from left): oxygen, superoxide, and chloride; third row: water/hydroxide with Tyr-244 deprotonated and protonated, and hydroxide/hydroxide; last row: water bound to iron, water bound to copper, and a linear combination of water/hydroxide and the one water model (see text). The structures were visualized in VMD [85].

3.1.1. Oxygenous species

Properties of the DFT optimized structures are summarized in Table 2 and some selected structures are shown in Fig. 2. Overall, the movement taking place in the quantum optimizations is not very large in any system of the binuclear site with bound O_2^{2-}, $O_2^{*/-}$, or O_2, having an overall root–mean–square deviation (RMSD) of ~0.4 Å or less for all non-hydrogen atoms as compared to the crystal structure. The main movement took place in the O–O distance of the ligand, some alteration in the heme planarity, as well as some alterations in the Tyr-244 orientation. In comparison to the oxygen–oxygen distance of 1.7 Å in the X-ray structure of Aoyama et al. [25], the bond length of the bound peroxide dianion is only 1.3 Å in the QM-optimized active site structure with peroxide. The resolution of the X-ray structure is 2 Å and Cruickshank's dispersion precision indicator (DPI) [54,55] is 0.14 Å. As a general rule of thumb, the accuracy of an X-ray structure is about one tenth of the resolution. The oxygen–oxygen bond length increases when protons are added to the peroxide. However, as the protonation state is increased, the peroxide becomes more loosely bound to the binuclear site, e.g. in the hydrogen peroxide (H_2O_2) structure, the Fe–O distance is 2.72 Å, indicating that the species is practically unbound. The Fe–Cu distance in the di- and monoanionic peroxide structures (O_2^{2-} and OOH^-) agree well (i.e. within 0.03–0.11 Å) with the refined X-ray structure, whereas the Fe–Cu distance in the hydrogen peroxide structures is 0.7 Å longer than that in the X-ray structure.

The O–O bond length of dioxygen bound to the binuclear site is 1.29 Å, similar to the O–O bond length of O_2^{2-} bound to the BNC (Table 2). The Fe–Cu distance of the binuclear site agrees very well with the crystal structure (see below). Gas-phase calculations at the BP86/def2-SVP level yielded bond lengths of 1.22 Å, 1.36 Å, and 1.63 Å for O_2, $O_2^{*/-}$, and O_2^{2-}, respectively (at B3LYP/def2-TZVP level, the respective bond lengths are 1.22 Å, 1.35 Å, and 1.60 Å). Free O_2^{2-} is not stable in the gas-phase. In the vicinity of an electron acceptor, it donates one electron to the environment. However, Rulísek et al [56]. showed that O_2^{2-} can be stabilized by the three coppers in multicopper oxidases. At the BP86/def2-SVP level of theory, the anionic peroxide

(OOH^-) and hydrogen peroxide (H_2O_2) species obtained by protonation of O_2^{2-} have bond lengths of 1.53 Å and 1.46 Å, respectively (at B3LYP/def2-TZVP level, the respective bond lengths are 1.53 Å and 1.47 Å). The O–O bond of both O_2 and O_2^{2-} bound to the BNC resembles the bond distance of $O_2^{*/-}$ obtained in the gas-phase calculation, indicating that the species confined between the metals has superoxide character. Similarly, the bound anionic peroxide has also a somewhat shorter O–O bond compared to the free form. For comparison, the structure of dioxygen bound to the reduced ferrous/cuprous binuclear site is also reported in Table 2, which shows a short O–O bond of 1.32 Å but a considerably shorter Fe–Cu distance of 4.10 Å.

In contrast to the peroxide and oxygen structures where the O–O distance is perturbed from the free gas-phase value, the O–O bond length observed in the superoxide structure is 1.32 Å and almost identical to the bond length of superoxide observed in gas-phase (1.35 Å). This indicates that the electronic structure of the superoxide will remain nearly identical to what is observed for the free species, which is also consistent with the spin and charge distribution (see below). The Fe–Cu distance of the superoxide structure fits with the experimental Fe–Cu distance very well.

3.1.2. Electronic structure of oxygenous species in the binuclear site

Spin densities of oxygen, superoxide, and dianionic peroxide bound to the binuclear site are shown in Fig. 3 and summarized in Table 3. In all three structures, the O–O moiety comprises almost a unit electron spin, suggesting that it effectively has superoxide character in agreement with the geometrical properties presented in Section 3.1.1. This finding is also in agreement with the general "rule" that the BNC prefers to bind singly negatively charged species [57]. The Mulliken charge of the O–O moiety varies between −0.34 e and −0.41 e in these structures, which resembles the RESP-charge of −0.5 e of a hydroxyl bound to a ferric heme [58]. The interpretation of spin distributions in the heme system is more complex. When the heme system is divided to the iron and the porphyrin parts, a unit spin is observed on the iron in the oxygen and superoxide structures, whereas two electron spins are observed on the iron in the dianionic peroxide structure. In addition, almost a unit spin is observed on the porphyrin moiety in the oxygen structure. Compared to the reduced and oxidized five-coordinated high-, intermediate-, and low-spin hemes (see Table 3), the superoxide and dianionic peroxide structures have spin distributions resembling a low-spin ferric heme and intermediate-spin ferrous heme, respectively. The oxygen structure has a more complex spin distribution, showing a porphyrin radical, which is also obtained for the high-spin heme model. Although the Mulliken population analysis is not very accurate, it qualitatively suggests that heme a_3 is oxidized in the oxygen and superoxide structures and reduced in the dianionic peroxide structure, in agreement with the geometrical properties of the systems discussed in Section 3.1.

Table 3
Spin densities of dioxygen, superoxide, and dianionic peroxide bound forms of the binuclear site, compared to the reduced and oxidized high-spin (HS), intermediate-spin (IS), and low-spin (LS) hemes. Fe indicates iron; Porph, porphyrin moiety + proximal histidine; L, the oxygenous ligand; Cu, copper; other, His-240, His-290, His-291, Tyr-244.

System	Fe	Porph	L	Cu	Other
O_2	1.1	0.7	−0.9	0.6	0.5
$O_2^{*/-}$	1.2	0.0	1.1	0.6	0.1
O_2^{2-}	2.4	−0.2	1.3	0.3	0.2
Spin density difference					
$O_2 - O_2^{*/-}$	−0.1	0.7	−2.0	0.0	0.4
$O_2^{2-} - O_2^{*/-}$	1.2	−0.2	0.2	−0.3	0.1
Charge density difference					
$O_2 - O_2^{*/-}$	0.0	0.6	0.0	0.0	0.4
$O_2^{2-} - O_2^{*/-}$	−0.3	−0.5	−0.1	0.0	−0.1
Heme Fe[II]					
HS	3.8	0.2	–	–	–
IS	2.1	−0.1	–	–	–
LS	0	0	–	–	–
Heme Fe[III]					
HS	4.2	0.8	–	–	–
IS	2.9	0.1	–	–	–
LS	1.2	−0.2	–	–	–

Subtracting the spin and charge densities of superoxide from the oxygen and dianionic peroxide, respectively, reveals how the excess electron delocalizes in these states (Fig. 4). Spin and charge density difference between oxygen and superoxide suggest that the electron will mainly pair with the unpaired porphyrin radical. In contrast, the spin density difference between dianionic peroxide and superoxide takes place mainly on the iron, suggesting that the heme is reduced in the former case, as concluded above.

This picture discussed above is also in agreement with geometrical properties of the systems. Reduced and oxidized high-spin hemes have significant structural differences [59]. Ferrous high-spin heme a_3 has an Fe–His bond length of 2.20 Å, whereas for ferric high-spin heme a_3, it is 2.10 Å. Although the bond length alters with the ligand in the distal position, this trend holds for all ferrous and ferric states. As shown in Table 2, the Fe–His bond length is 2.3 Å in the dianionic peroxide structure, whereas it is 2.01–2.02 Å for the oxygen and superoxide bound forms. The longer Fe–His bond in the former state indicates that the peroxide dianion has reduced the heme, whereas it remains oxidized in the oxygen and superoxide bound states. This picture is in agreement with the computed spin and charge densities.

These observations imply that if a dianionic peroxide would bind to the oxidized binuclear center, it would reduce heme a_3. Aoyama et al. [25] observed spectral features characteristic for an oxidized

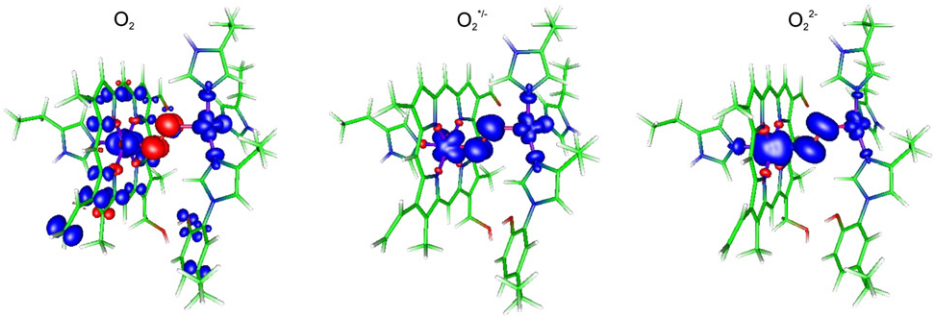

Fig. 3. Spin density of O_2 (above), superoxide (middle), and peroxide (below). Isocontour surfaces of +0.005 e and −0.005 e are shown in blue and red, respectively. The figure was prepared with gOpenMol [86].

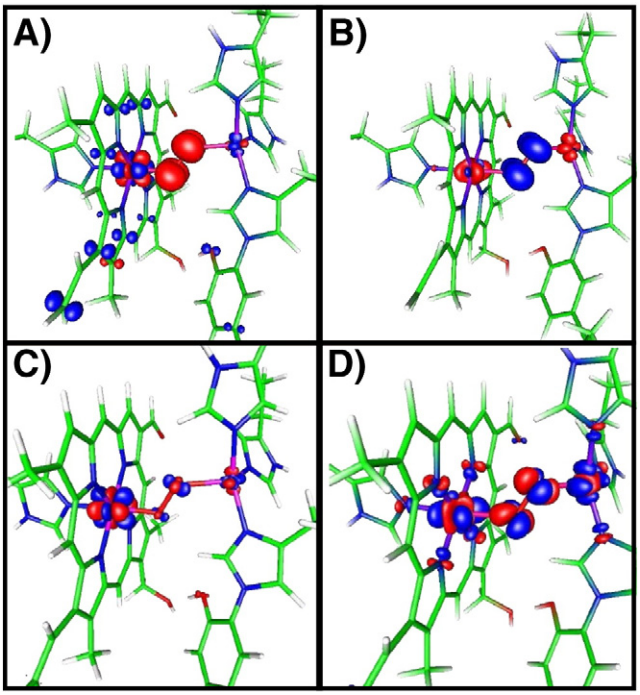

Fig. 4. Spin and charge density differences. Spin density difference between A) O_2 and superoxide and B) dianionic peroxide and superoxide. Charge density differences between C) O_2 and superoxide and D) dianionic peroxide and superoxide. Isocontour surfaces of +0.05 e and −0.05 e are shown in blue and red, respectively. The figure was prepared with gOpenMol [86].

binuclear site, which suggests that dioxygen or superoxide are better candidates for the observed species.

3.1.3. Hydrogen-bonded structures and linear combinations of different aqueous species

DFT calculations on hydrogen-bonded structures, i.e. two hydroxides or a hydroxide and a water molecule, yield shortest O–O distance of 2.47 Å. As pointed out by Aoyama et al. [25], the shortest O–O distance of a hydrogen-bonded structure in the Cambridge Structural Database is 2.4 Å, which agrees well with our structures. Interestingly, the short bond length of 2.47 Å falls within the classification of low-barrier hydrogen bonds (LBHB) [60]. Such bonds, in which the proton transfer reaction has very low activation energy, have been argued to play an important role in enzyme catalysis [60,61] (but cf. also reference 62). Interestingly, the ligand structure is affected by the protonation state of Tyr-244. When deprotonated, the copper binds water whereas the iron binds a hydroxide and vice versa when Tyr-244 is protonated. This effect is probably due to the increased Cu[I]/Tyr-O^* character of the Cu[II]-H_2O structure when Tyr-244 is deprotonated [10]. When two hydroxides are bound to the BNC, the O–O distance increases to 2.65–2.75 Å, which is characteristic for a normal hydrogen bond. Similarly, the oxo-hydroxy (O^{2-}/OH^-) ligand combination has an O–O distance of 2.65–2.75 Å.

When two water molecules are optimized in the oxidized BNC, one of them dissociates during the optimization, indicating that the BNC will probably not bind two water molecules (see also Koepke et al. [26]).

A third possibility is one water/hydroxide molecule tumbling between the two metals. The dynamic motion of the molecule would statistically give rise a short apparent O–O distance. A linear combination of two water molecules would indeed give rise to a O–O distance of 1.98 Å and 1.47 Å when Tyr-244 is protonated or deprotonated, respectively (Table 2). Energetically, the water prefers to bind to the copper with −3.8 kcal/mol and −2.4 kcal/mol at B3LYP/def2-TZVP level of theory, in the respective protonation states of Tyr-244. Considering the error limit of the computational method, this difference could be sufficient to see a significant population of water on both metals.

3.1.4. Chloride (Cl^-)

In X-ray studies, a chloride anion can be considered to be isoelectronic with O_2 and might therefore give rise to an electron density map similar to dioxygen. A chloride binds well to the oxidized BNC as indicated by the short Fe–Cl and Cu–Cl distance of 2.55 Å and 2.41 Å, respectively. The Fe–Cu distance of 4.58 Å of the chloride structure also agrees well with the Fe–Cu distance observed in the refined X-ray structure. Bromide substitution was used to study if the electron density could account for chloride (see below). According to our calculations, bromide also seems to bind well to the oxidized BNC, albeit ~10 kcal/mol less favorable than chloride. The bromide structure resembles the chloride structure, with Fe–Br and Cu–Br distance of 2.81 Å and 2.48 Å, respectively. The Fe–Cu distance of 4.66 Å is also very similar to the one obtained for the chloride structure.

3.2. Comparison of DFT structures with the experimental electron density

The QM-optimized structures of the binuclear site with bound O_2^{2-}, $O_2^{*/-}$, and O_2 were all found to fit well with the experimental electron density, despite the short O–O distances. This indicates that all these species could structurally account for the electron density observed between the metals. Fig. 5A shows negligible mF_o–DF_c density, for a species with an O–O distance of 1.3 Å obtained from the QM-optimized structure. Although the resolution of the X-ray density is not high enough to structurally distinguish between peroxide, superoxide, and oxygen, the structural accuracy of DFT is estimated to be 0.05 Å. As suggested in Section 3.1.2, based on comparison between the isolated reduced and oxidized hemes and the oxygenous structures, the peroxide dianion has reduced the heme, whereas it remains oxidized in the oxygen and superoxide bound states.

Neither the two water model nor the one water model discussed above are very consistent with the X-ray data. When the equivalent of two oxygen atoms (H_2O/OH^- or H_2O/H_2O) is placed between the metals, a positive density (~5 σ) remains in the mF_o–DF_c map (Fig. 5B). When the equivalent of only one oxygen atom is placed between the metals, significant positive density (>5 σ) also remains in the mF_o–DF_c map (Fig. 5C). This indicates that the 8 electrons of a water molecule are not sufficient to account for the scattering. The number of scattering electrons increases if the oxygenous species would consist of a mixture of H_2O/OH^- and one water molecule; with a half-and-half mixture of these species, the O–O bond would increase to 1.97 Å and the oxygenous species would statistically contribute 12 scattering electrons. Such a species could originate from the protonation of hydroxide in the H_2O/OH^- species, leading to dissociation of one water molecule (see above). However, despite the theoretical feasibility of such a model, it did not fit the experimental density very well as shown in Fig. 5D.

A chloride anion bound to the binuclear site was also considered. The chloride structure fits the experimental electron density (Fig. 5E), as previously concluded by Koepke et al. [26]. Aoyama et al. [25] argued that the observed elliptic electron density makes chloride an unlikely candidate as this species is expected to give rise to a more spherical density distribution. However, at 2 Å resolution, the shape of an electron density peak is not a very conclusive evidence, especially given that Aoyama et al. [25] had refined the anisotropic displacement factors for the metal ions, which further complicates the interpretation of the electron density between the two heavy metal scatterers. Chloride seems to describe the density relatively well (Fig. 5E), probably due to the close proximity of the metals. Koepke et al. [26] tested the chloride hypothesis by substituting all chloride buffers with analogous bromide buffers. This substitution did not alter the observed

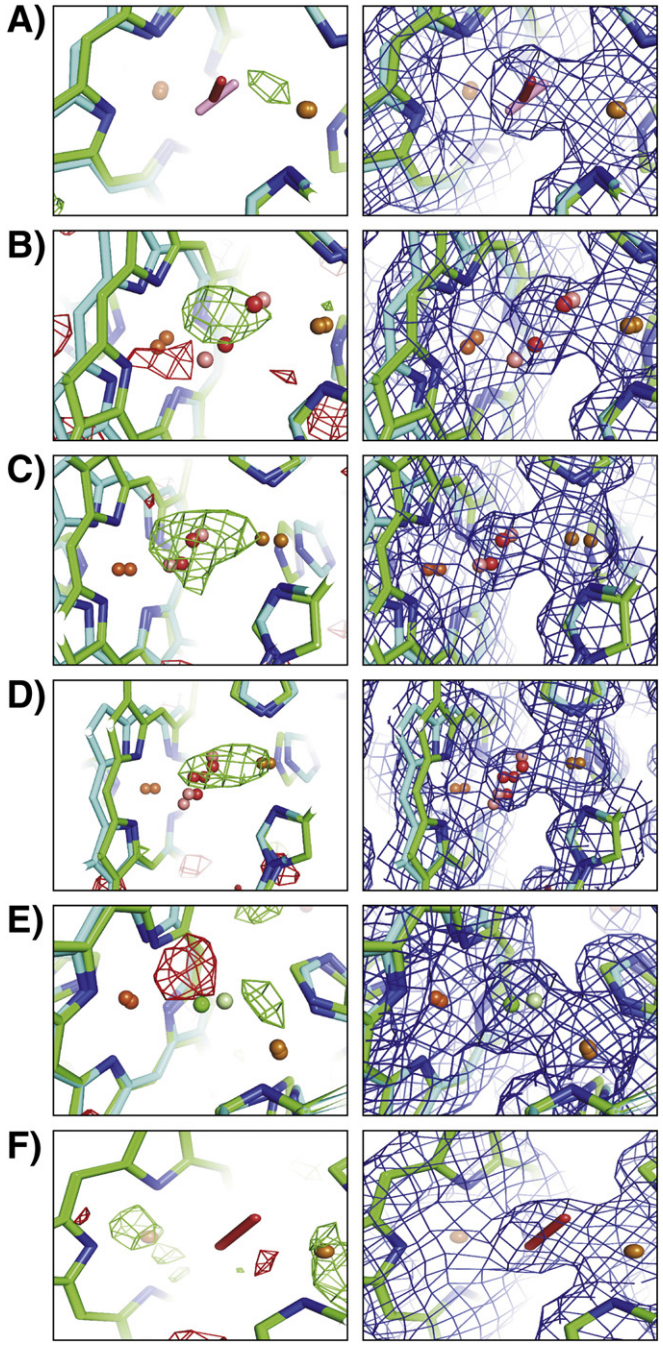

Fig. 5. A comparison of the DFT-calculated structures with the structures refined against the X-ray data. A) Peroxide/superoxide/oxygen structures (O–O distance, 1.3 Å); B) water/hydroxyl structure (O–O distance, 2.5 Å); C) linear combination of two water molecules with a 50% population on each metal (O–O distance, 1.5 Å); D) linear combination of 50% one water model (O–O distance, 1.47 Å) and a 50% water + hydroxyl structure (O–O distance, 2.5 Å); E) chloride ion; F) the original crystal structure of Aoyama et al. [25]. The calculated structure is shown with carbons (cyan), oxygen (pink), and chloride (light green) while the structure refined against X-ray data is shown with carbons (green) and oxygen (red). The $2mF_o$-DF_c maps (blue) are contoured at 1 σ and the positive (green) and negative (red) mF_o-DF_c maps at 3 σ. The crystallographic re-refinement was based on the DFT structures with the shortest O–O distances and/or Fe–Cu distance, i.e. in A) the O_2-bound structure with Tyr-244 deprotonated and in B–F) the structures with Tyr-244 deprotonated (cf. Table 2).

electron density, and it was concluded that dianionic peroxide (O_2^{2-}) is a more likely candidate than chloride. Our calculations indicate that bromide can also bind very tightly to the BNC (Table 2), resembling the chloride bound structures. The argument that bromide may be too large is not feasible as the difference in ionic radii between bromide and chloride is only 0.15 Å, which is much less than typical average root–mean–square fluctuations of conduction pores in proteins [63]. Interestingly, despite the relatively similar geometries of the two halogen structures, we observed a large binding energy difference between chloride and bromide of ~10 kcal/mol, which might explain the discrimination between the two halogens. This might also explain why Ralle et al. [64] could not successfully remove chloride by bromide substitution nor by extensive dialysis of the *Escherichia coli* cytochrome bo_3 enzyme. The strongest argument against chloride, however, seems to be that the electron density between the BNC metals failed to yield anomalous scattering from chloride under conditions where such scattering was observed for sulfur atoms (S. Yoshikawa, personal communication). This suggests that there could be no more than about 10% chloride in the active site.

3.3. Energetic aspects

As concluded in the previous section, dioxygen fits well in the observed electron density, just as well as dianionic peroxide and superoxide. However, considering the relatively poor affinity for O_2 to the fully reduced binuclear site (K_d ~0.3 mM; [65]), this hypothesis might seem unfeasible, particularly when considering that a ferric heme has no affinity for oxygen. To test oxygen binding to an oxidized BNC, the oxygen affinity was calculated and compared with the oxygen affinity of a reduced and oxidized A-type heme with a proximal histidine as well as to a reduced BNC. Radon and Pierloot [68] have shown that absolute oxygen binding energies depend on the employed density functional, whereas relative differences are more reliable. Moreover, Siegbahn et al. [38] have recently suggested the importance of dispersive effects for binding of small molecules to metal centers. Conventional DFT methods fail to describe such effects, but as shown by Grimme [39,40], these can be incorporated by introduction of an empirical $1/r^6$-correction term. Table 4 summarizes the electronic binding energies of O_2 to the different models and states and clearly verifies both important computational aspects. As DFT fails to describe the energetics of open-shell singlet species [66], a Heisenberg J/2 value [67] of ~3 kcal/mol as estimated by Blomberg et al. [66] has been subtracted from the O_2-binding energies of systems with a ferrous heme. To approximate binding free energies from the electronic energies, the values must be corrected for the binding entropy of a diatomic molecule, which will increase the free energies by ~10 kcal/mol [66,69]. Moreover, the μM-dioxygen concentration typical for tissues [70] will further increase the binding free energy. Considering the electronic energies shown in Table 4 and the above approximations, the binding free energy of O_2 will indeed be slightly exergonic when Tyr-244 is protonated and nearly isergonic with dioxygen binding to a reduced BNC. At equilibrium, this would most probably be sufficient to populate the BNC with oxygen. However, it must be emphasized that dioxygen is kinetically trapped to the reduced binuclear center, which alters the apparent Michaelis

Table 4
Electronic O_2-binding energies to an oxidized and reduced BNC and to a ferrous and ferric heme obtained with different density functionals. The computational methods are the Becke–Parr-86 gradient generalized functional (BP86), the dispersion corrected BP86 (D-BP86), Becke's hybrid three-parameter functional (B3LYP), the dispersion corrected B3LYP (D-B3LYP), and D-B3LYP with a dielectric constant set to 4 (D-B3LYP/$\varepsilon = 4$). The ferrous heme energies were corrected with the Heisenberg J/2-value of 3 kcal/mol, as estimated by Blomberg et al. [66]. All energies are given in kilocalorie per mole.

System	Tyr	BP86	D-BP86	B3LYP	D-B3LYP	D-B3LYP/$\varepsilon = 4$
Heme Fe[II]	–	−28.7	−38.8	+10.6	+0.7	−1.9
Heme Fe[III]	–	−15.1	−24.8	+18.8	+9.2	+7.5
Fe[II]/Cu[I]	YOH	−23.5	−34.8	+0.6	−10.6	−11.9
Fe[III]/Cu[II]	YOH	−9.6	−25.3	+6.8	−12.4	−13.6
Fe[III]/Cu[II]	YO^-	−7.8	−21.4	+10.1	−3.4	−6.0

constant for dioxygen binding to the sub-μM regime [65], a factor that might be very different for the oxidized enzyme. In comparison, a free heme has a much lower affinity for O_2 even in its reduced form. For an oxidized heme, binding of O_2 is endergonic by ~20 kcal/mol. In comparison to e.g. hemoglobin or myoglobin, Blomberg et al. estimated that a distal histidine reduces this binding energy by ~10 kcal/mol [66], which would make binding of oxygen to myoglobin/hemoglobin favorable in the reduced state but highly non-favorable in the oxidized state. Despite the computational challenges and approximations used, the computed values clearly indicate that an oxidized BNC binds oxygen much stronger than an isolated heme.

The apparent pK_a of Tyr-244 has been estimated to be 6.5 in the oxidized enzyme from *Paracoccus denitrificans* [20]. A survey of crystallization conditions with enzyme from this source, from *R. sphaeroides* [25] and bovine heart [26], shows that crystallization was conducted at a pH well below 7. Hence, the protonated form of Tyr-244 would be expected to prevail in all these cases. Our calculations indicate that the binding of O_2 to the oxidized site is significant when Tyr-244 is protonated, which is consistent with the crystal structure work. If the species has resulted from dioxygen, we predict that at a higher pH, the oxygenous species observed in the BNC might disappear or, possibly, that the O–O distance would increase as the natural H_2O/OH^- ligand might substitute the oxygen.

A strong argument against the dianionic peroxide comes from the catalytic properties of the BNC. The oxidized BNC is known to react with hydrogen peroxide (H_2O_2), which leads to O–O bond splitting and formation of the P_M state [16,17]. Our preliminary calculations indicate that P_M, i.e. Fe[IV] = O^{2-} Cu[II]-OH^- Tyr-O^* is ~7 kcal/mol more stable than the ferric/cupric state with bound monoanionic peroxide (OOH^-). Similar conclusions were reached by Blomberg et al. [42,71–73] in extensive quantum chemical studies on the dioxygen splitting mechanism of C*c*O.

There are many synthetic analogs of the heme–copper BNC (cf. reference [74] for review). The only known μ-peroxo-bridged binuclear coordination complex, [(TMP)Fe[III]-(O_2^{2-})-(5MeTPA)-Cu[II]]$^+$, shows μ-η_2:η_1 binding of a dianionic peroxide [75], in contrast to μ-1,2 binding observed in C*c*O and as judged from our calculations. As discussed by Kim et al. [74], there are several structural differences between this and other known peroxo-bridged coordination analogs and the structural properties of the BNC in C*c*O. For example, the iron–copper distance, which can experimentally be accurately determined, is 3.92 Å in the synthetic dianionic peroxide structure, while the X-ray structure of C*c*O has an Fe–Cu distance of 4.9 Å. On this basis, Kim et al. [74] excluded binding of a dianionic peroxide to the oxidized BNC of C*c*O, and similar to our conclusions, it was suggested that dioxygen might be a possible ligand candidate.

For studying oxygen binding to an oxidized BNC, the optical spectra of oxygenated and fully oxidized anaerobic enzyme were carefully measured, but no spectral difference was observed (Fig. 6). The analysis of spin and charge densities of dioxygen bound to the BNC suggests that the oxidation state of heme a_3 remains unchanged. Therefore, it is plausible that the UV–VIS spectrum of heme a_3 does not change upon oxygen binding in the oxidized state, while it also remains possible that dioxygen does not bind to the oxidized BNC in the experimental conditions.

Our calculations indicate that irrespective of whether dianionic peroxide, superoxide, or dioxygen is inserted in the oxidized BNC, the resulting ligand gains superoxide character. The picture of superoxide stabilization is in agreement with the general view that the BNC prefers to bind a singly negatively charged species such as cyanide, formate, chloride, azide, and hydroxide, a conclusion also theoretically found to apply for different heme models [76]. Mitchell and Rich [77] have pointed out that the BNC ligands most likely diffuse into the active site of C*c*O in their neutral forms, after which they deprotonate and bind. Since chloride can be excluded (see above), a molecular species with two oxygen atoms is the best candidate for explaining the observed structure. Dianionic peroxide can most likely be excluded based on its reactivity (see above), but superoxide and dioxygen remain possible candidates. Due to relatively rapid freezing and the extremely slow diffusion in the cryo-cooled state, O_2 is presumably bound to the oxidized BNC before freezing, consistent with our energetic calculations (see above). Synchrotron radiation may readily reduce bound O_2 to superoxide, similar to other observed synchrotron radiation induced changes, such as cleavage of disulphide bridges [78]. Indeed, reduction of redox enzyme active sites by synchrotron radiation is frequently observed e.g. in references [79] and [80]. Whatever the mechanism, our data suggest that the oxidized BNC stabilizes the superoxide form even though O_2 is formally the ligand.

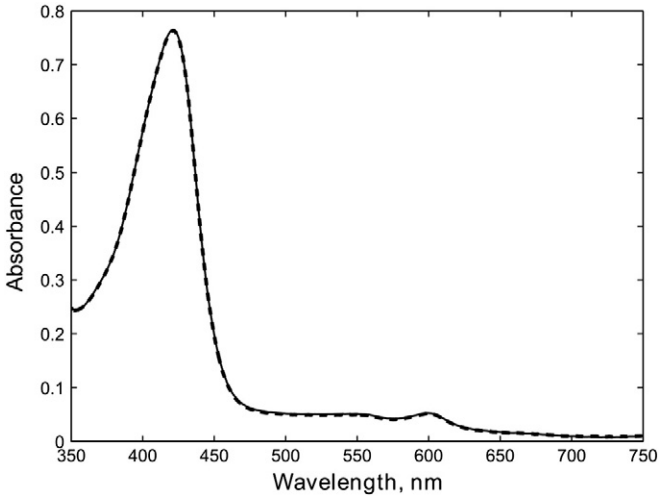

Fig. 6. Optical spectra of oxidized bovine C*c*O (concentration 4.2 μM) measured in anaerobic (full line) and aerobic (dotted line) conditions. Medium: 100 mM of MES-buffer (pH 6.5); DDM, 0.15%.

Finally, we consider whether the catalytic cycle of C*c*O might involve a stable peroxide state, in which the peroxide bond is intact or if the catalytic properties of C*c*O will result in its immediate scission producing two (unprotonated) water molecules. Early studies of C*c*O supported the former hypothesis. ATP-induced reversal of the catalytic cycle of C*c*O in mitochondria led to two electron donation to a redox buffer from the oxidized BNC plus water [81], forming the P_M state which could also be formed with hydrogen peroxide (see Introduction). However, beginning with the optical study of Weng and Baker [82], and followed up by Raman [83] and isotope labeling studies [84], it is now known with certainty that the O–O bond is cleaved in the P_M state.

4. Conclusions

We have demonstrated here by combined high-level quantum chemical calculations and analysis of the experimental X-ray data that the recently found oxygenous species confined between the metals in the oxidized binuclear site of C*c*O most probably has superoxide character. The bound species probably originates from dioxygen bound to the site and is presumably reduced to superoxide by electrons produced by the synchrotron radiation. The resolution of the X-ray map is not sufficient to distinguish between a dianionic peroxide, superoxide, and oxygen—all species fitting equally well in the electron density. Analysis of the geometries and electronic structures of these species make it unlikely that the bound species is the peroxide dianion, which is expected to lead to formation of the catalytic P_M intermediate. In contrast to an oxidized A-type heme, which has no affinity for dioxygen, we find that binding of dioxygen to the oxidized binuclear site is weakly exergonic. In agreement with Aoyama et al. [25] and Koepke et al. [26], we conclude that hydrogen-

bonded structures have too long O–O distance and therefore do not satisfy the experimental data, neither does a mixture of different aqueous ligands.

Acknowledgments

This research has been supported by HENAKOTO, the Academy of Finland (MW), the Sigrid Jusélius Foundation, as well as by the Academy of Finland through its Centers of Excellence Programme 2006–2011 (DS). EO acknowledges the National Graduate School in Informational and Structural Biology for funding. CSC, the Finnish IT Center for Science, is acknowledged for computer time. MW is grateful to Dr. Shinya Yoshikawa and Dr. Margareta Blomberg for discussions.

References

[1] G.T. Babcock, How oxygen is activated and reduced in respiration, Proc. Natl. Acad. Sci. U. S. A. 96 (1999) 12971–12973.
[2] M. Wikström, Proton pump coupled to cytochrome-c oxidase in mitochondria, Nature 266 (1977) 271–273.
[3] M. Wikström, M.I. Verkhovsky, Mechanism and energetics of proton translocation by the respiratory heme–copper oxidases, Biochim. Biophys. Acta 1767 (2007) 1200–1214.
[4] V.R.I. Kaila, M.I. Verkhovsky, M. Wikström, Proton-coupled electron transfer in cytochrome oxidase, Chem. Rev. 110 (2010) 7062–7081.
[5] G.T. Babcock, M. Wikström, Oxygen activation and the conservation of energy in cell respiration, Nature 356 (1992) 301–309.
[6] J.F. Turrens, Mitochondrial formation of reactive oxygen species, J. Physiol. 552 (2003) 335–344.
[7] S. Yoshikawa, K. Shinzawa-Itoh, R. Nakashima, R. Yaono, E. Yamashita, N. Inoue, M. Yao, M.J. Fei, C.P. Libeu, T. Mizushima, H. Yamaguchi, T. Tomizaki, T. Tsukihara, Redox-coupled crystal structural changes in bovine heart cytochrome *c* oxidase, Science 280 (1998) 1723–1729.
[8] K.M. McCauley, J.M. Vrtis, J. Dupont, W.A. van der Donk, Insights into the functional role of the tyrosine–histidine linkage in cytochrome *c* oxidase, J. Am. Chem. Soc. 122 (2000) 2403–2404.
[9] Y. Bu, R.I. Cukier, Structural character and energetics of tyrosyl radical formation by electron/proton transfers of a covalently linked histidine–tyrosine: a model for cytochrome *c* oxidase, J. Phys. Chem. B 109 (2005) 22013–22026.
[10] V.R.I. Kaila, M.P. Johansson, D. Sundholm, L. Laakkonen, M. Wikström, The chemistry of the Cu_B site in cytochrome *c* oxidase and the importance of its unique His-Tyr bond, Biochim. Biophys. Acta – Bioenergetics 1787 (2009) 221–233.
[11] B. Chance, C. Saronio, J.S. Leigh, Functional intermediates in the reaction of membrane bound cytochrome oxidase with oxygen, J. Biol. Chem. 250 (1975) 9226–9237.
[12] K.P. Jensen, B.O. Roos, U. Ryde, O_2-binding to heme: electronic structure and spectrum of oxyheme, studied by multiconfigurational methods, J. Inorg. Biochem. 99 (2005) 45–54.
[13] K. Jensen, U. Ryde, How O_2 binds to heme—reasons for rapid binding and spin inversion, J. Mol. Biol. 279 (2004) 14561–14569.
[14] D.A. Proshlyakov, M.A. Pressler, G.T. Babcock, Dioxygen activation and bond cleavage by mixed-valence cytochrome *c* oxidase, Proc. Natl Acad. Sci. U. S. A. 95 (1998) 8020–8025.
[15] D.A. Proshlyakov, M.A. Pressler, C. DeMaso, J.F. Leykam, D.L. DeWitt, G.T. Babcock, Oxygen activation and reduction in respiration: involvement of redox-active tyrosine 244, Science 290 (2000) 1588–1591.
[16] J.M. Wrigglesworth, Formation and reduction of a peroxy intermediate of cytochrome-c oxidase by hydrogen-peroxide, Biochem. J. 217 (1984) 715–719.
[17] S. Junemann, P. Heathcote, P.R. Rich, The reactions of hydrogen peroxide with bovine cytochrome *c* oxidase, Biochim. Biophys. Acta 1456 (2000) 56–66.
[18] P.R. Rich, M. Iwaki, A comparison of catalytic site intermediates of cytochrome *c* oxidase and peroxidases, Biochemistry (Moscow) (2007) 1047–1055.
[19] D. Jancura, V. Berka, M. Antalik, J. Bagelova, R.B. Gennis, G. Palmer, M. Fabian, Spectral and kinetic equivalence of oxidized cytochrome *c* oxidase as isolated and activated by reoxidation, J. Biol. Chem. 281 (2006) 30319–30325.
[20] E.A. Gorbikova, I. Belevich, M. Wikström, M.I. Verkhovsky, The proton donor for O–O bond scission by cytochrome *c* oxidase, Proc. Natl Acad. Sci. U. S. A. 105 (2008) 10733–10737.
[21] M.I. Verkhovsky, A. Jasaitis, M.L. Verkhovskaya, J.E. Morgan, M. Wikström, Proton translocation by cytochrome *c* oxidase, Nature 400 (1999) 480–483.
[22] D. Bloch, I. Belevich, A. Jasaitis, C. Ribacka, A. Puustinen, M.I. Verkhovsky, M. Wikström, The catalytic cycle of cytochrome *c* oxidase is not the sum of its two halves, Proc. Natl Acad. Sci. U. S. A. 101 (2004) 529–533.
[23] M. Ruitenberg, A. Kannt, E. Bamberg, B. Ludwig, H. Michel, K. Fendler, Single-electron reduction of the oxidized state is coupled to proton uptake via the K pathway in *Paracoccus denitrificans* cytochrome *c* oxidase, Proc. Natl Acad. Sci. U. S. A. 97 (2000) 4632–4636.
[24] V.R.I. Kaila, M.I. Verkhovsky, G. Hummer, M. Wikström, Mechanism and energetics by which glutamic acid 242 prevents leaks in cytochrome *c* oxidase, Biochim. Biophys. Acta Bioenerg. 1787 (2009) 1205–1214.
[25] H. Aoyama, K. Muramoto, K. Shinzawa-Itoh, K. Hirata, T. Yamashita, E. Tsukihara, T. Ogura, S. Yoshikawa, A peroxide bridge between Fe and Cu ions in the O_2 reduction site of fully oxidized cytochrome *c* oxidase could suppress the proton pump, Proc. Natl Acad. Sci. U. S. A. 106 (2009) 2165–2169.
[26] J. Koepke, E. Olkhova, H. Angerer, H. Müller, G. Peng, H. Michel, High resolution crystal structure of *Paracoccus denitrificans* cytochrome *c* oxidase: new insights into the active site and the proton transfer pathways, Biochim. Biophys. Acta Bioenerg. 1787 (2009) 635–645.
[27] A.D. Becke, Density-functional exchange-energy approximation with correct asymptotic behavior, Phys. Rev. A 38 (1988) 3098–3100.
[28] J.P. Perdew, Density-functional approximation for the correlation energy of the inhomogeneous electron gas, Phys. Rev. B 34 (1986) 8822–8824.
[29] K.P. Jensen, B.O. Roos, U. Ryde, Performance of density functionals for first row transition metal systems, J. Chem. Phys. 126 (2007) 1–14, 014103.
[30] M. Sierka, A. Hogekamp, R. Ahlrichs, Fast evaluation of the Coulomb potential for electron densities using multipole accelerated resolution of identity approximation, J. Chem. Phys. 118 (2003) 9136–9148.
[31] A. Schäfer, H. Horn, R. Ahlrichs, Fully optimized contracted Gaussian basis sets for atoms Li to Kr, J. Chem. Phys. 97 (1992) 2571–2577.
[32] F. Weigend, R. Ahlrichs, Balanced basis sets of split valence, triple zeta valence and quadruple zeta valence quality for H to Rn: design and assessment of accuracy, Phys. Chem. Chem. Phys. 7 (2005) 3297–3305.
[33] A.D. Becke, Density-functional thermochemistry. III. The role of exact exchange, J. Chem. Phys. 98 (1993) 5648–5652.
[34] C. Lee, W. Yang, R.G. Parr, Development of the Colle–Salvetti correlation-energy formula into a functional of the electron density, Phys. Rev. B 37 (1988) 785–789.
[35] L.A. Curtiss, K. Raghavachari, G.W. Trucks, J.A. Pople, Gaussian-2 theory for molecular energies of first- and second-row compounds, J. Chem. Phys. 94 (1991) 7221–7230.
[36] L.A. Curtiss, K. Raghavachari, R.C. Redfern, J.A. Pople, Assessment of Gaussian-3 and density functional theories for a larger experimental test set, J. Chem. Phys. 112 (2000) 7374–7383.
[37] P.E.M. Siegbahn, M.R.A. Blomberg, Density functional theory of biologically relevant metal centers, Annu. Rev. Phys. Chem. 50 (1999) 221–249.
[38] P.E.M. Siegbahn, M.R.A. Blomberg, S.-L. Chen, Significant van der Waals effects in transition metal complexes, J. Chem. Theory Comput. 6 (2010) 2040–2044.
[39] S. Grimme, Accurate description of van der Waals complexes by density functional theory including empirical corrections, J. Comput. Chem. 25 (2004) 1463–1473.
[40] S. Grimme, Semiempirical GGC-type density functional constructed with a long-range dispersion contribution, J. Comput. Chem. 27 (2006) 1787–1799.
[41] A. Klamt, G. Schüürmann, COSMO: a new approach to dielectric screening in solvents with explicit expressions for the screening energy and its gradient, J. Chem. Soc. Perkin Trans. 2 (1993) 799–805.
[42] M.R.A. Blomberg, P.E.M. Siegbahn, G.T. Babcock, M. Wikström, Modeling cytochrome oxidase: a quantum chemical study of the O–O bond cleavage mechanism, J. Am. Chem. Soc. 122 (2000) 12848–12858.
[43] A. Ghosh, P.R. Taylor, High-level ab initio calculations on the energetics of low-lying spin states of biologically relevant transition metal complexes: first progress report, Curr. Opin. Chem. Biol. 7 (2003) 113–124.
[44] A. Ghosh, Transition metal spin state energetics and noninnocent systems: challenges for DFT in the bioinorganic arena, J. Biol. Inorg. Chem. 11 (2006) 712–724.
[45] R. Ahlrichs, M. Bär, H. Häser, M. Horn, C. Kölmel, Electronic-structure calculations on workstation computers—the program system TURBOMOLE, Chem. Phys. Lett. 162 (1989) 165–169.
[46] G.N. Murshudov, A.A. Vagin, E.J. Dodson, Refinement of macromolecular structures by the maximum-likelihood method, Acta Cryst. D53 (1997) 240–255.
[47] R.J. Read, Improved Fourier coefficients for maps using phases from partial structures with errors, Acta Crystallogr. A 42 (1986) 140–149.
[48] P. Emsley, K. Cowtan, Coot: model-building tools for molecular graphics, Acta Cryst. D60 (2004) 2126–2132.
[49] W.L. DeLano, The PyMOL Molecular Graphics System, DeLano Scientific, San Carlos, CA, USA, 2002, http://www.pymol.org.
[50] S. Bailey, The CCP4 suite, Acta Cryst. 50 (1994) 760–763.
[51] U. Ryde, K. Nilsson, Quantum chemistry can locally improve protein crystal structures, J. Am. Chem. Soc. 125 (2003) 14232–14233.
[52] A.T. Brünger, et al., Crystallography & NMR system: a new software suite for macromolecular structure determination, Acta Cryst. D54 (1998) 905–921.
[53] A.T. Jones, J.Y. Zou, S.W. Cowan, M. Kjeldgaard, Improved methods for building protein models in electron density maps and the location of errors in these models, Acta Cryst. A47 (1991) 110–119.
[54] D.W.J. Cruickshank, The required precision of intensity measurements for single-crystal analysis, Acta Cryst. 13 (1960) 774–777.
[55] D.W.J. Cruickshank, Refinement of Macromolecular StructuresProceedings of CCP4 Study Weekend, 1996, pp. 11–22.
[56] L. Rulísek, E.I. Solomon, U. Ryde, A combined quantum and molecular mechanical study of the O_2 reductive cleavage in the catalytic cycle of multicopper oxidases, Inorg. Chem. 44 (2005) 5612–5628.
[57] M. Wikström, K. Krab, M. Saraste, Cytochrome oxidase - A synthesis, Academic Press.
[58] M.P. Johansson, V.R.I. Kaila, L. Laakkonen, Charge parameterization of the metal centers in cytochrome *c* oxidase, J. Comput. Chem. 29 (2008) 753–767.
[59] C. Rovira, K. Kunc, J. Hutter, P. Ballone, M. Parrinello, Equilibrium geometries and electronic structure of iron–porphyrin complexes: a density functional study, J. Phys. Chem. A 101 (1997) 8914–8925.
[60] C.L. Perrin, J.B. Nielson, "Strong" hydrogen bonds in chemistry and biology, Annu. Rev. Phys. Chem. 48 (1997) 511–544.

[61] W.W. Cleland, M.M. Kreevoy, Low-barrier hydrogen bonds and enzymic catalysis, Science 264 (1994) 1887–1890.
[62] A. Warshel, A. Papazyan, Energy considerations show that low-barrier hydrogen bonds do not offer a catalytic advantage over ordinary hydrogen bonds, Proc. Natl Acad. Sci. U. S. A. 93 (1996) 13665–13670.
[63] S.Y. Noskov, S. Berneche, B. Roux, Control of ion selectivity in potassium channels by electrostatic and dynamic properties of carbonyl ligands, Nature 431 (2004) 830–834.
[64] M. Ralle, M.L. Verkhovskaya, J.E. Morgan, M.I. Verkhovsky, M. Wikström, N.J. Blackburn, Coordination of Cu_B in reduced and CO-liganded states of cytochrome bo_3 from *Esherichia coli*. Is chloride ion a cofactor? Biochemistry 38 (1999) 7185–7194.
[65] M.I. Verkhovsky, J.E. Morgan, A. Puustinen, M. Wikström, Kinetic trapping of oxygen in cell respiration, Nature 380 (1996) 268–270.
[66] L.M. Blomberg, M.R.A. Blomberg, P.E.M. Siegbahn, A theoretical study on the binding of O_2, NO and CO to heme proteins, J. Inorg. Biochem. 99 (2005) 949–958.
[67] L. Noodleman, D.A. Case, Density-functional theory of spin polarization and spin coupling in iron–sulfur clusters, Adv. Inorg. Chem. 38 (1992) 423–470.
[68] M. Radon, K. Pierloot, Binding of CO, NO, and O_2 to heme by density functional and multireference ab initio calculations, J. Phys. Chem. A 112 (2008) 11824–11832.
[69] For example, $T\Delta S$ at 310 K for the reaction $Fe[II][NH_3]_3 + O_2 \rightarrow Fe[II][NH_3]_3\text{-}O_2$ at B3LYP/SV(P) level of theory is -12.1 kcal/mol, which compares well with the values reported in ref. [66].
[70] O. Ndubuizu, J.C. LaManna, Brain tissue oxygen concentration measurements, Antioxid. Redox Signaling 9 (2007) 1207–1219.
[71] M.R.A. Blomberg, P.E.M. Siegbahn, G.T. Babcock, M. Wikström, O–O bond splitting mechanism in cytochrome oxidase, J. Inorg. Biochem. 80 (2000) 261–269.
[72] M.R.A. Blomberg, P.E.M. Siegbahn, M. Wikström, Metal-bridging mechanism for O–O bond cleavage in cytochrome C oxidase, Inorg. Chem. 42 (2003) 5231–5243.
[73] M.R.A. Blomberg, P.E.M. Siegbahn, Quantum chemistry as a tool in bioenergetics, Biochim. Biophys. Acta 1797 (2010) 129–142.
[74] E. Kim, E.E. Chufán, L. Kamaraj, K.D. Karlin, Synthetic models for heme–copper oxidases, Chem. Rev. 104 (2004) 1077–1133.
[75] T. Chishiro, Y. Shimazaki, F. Tani, Y. Tachi, Y. Naruta, S. Karasawa, S. Hayami, Y. Maeda, Isolation and crystal structure of a peroxo-bridged heme–copper complex, Angew. Chem., Int. Ed. 42 (2003) 2788–2791.
[76] P. Rydberg, E. Sigfridsson, U. Ryde, On the role of the axial ligand in heme proteins: a theoretical study, J. Biol. Inorg. Chem. 9 (2004) 203–223.
[77] R. Mitchell, P.R. Rich, Proton uptake by cytochrome *c* oxidase on reduction and on ligand binding, Biochim. Biophys. Acta 28 (1994) 19–26.
[78] M. Weik, R.G.B. Ravelli, G. Kryger, S. McSweeney, M.L. Raves, M. Harel, P. Gros, I. Silman, J. Kroon, J.L. Sussman, Specific chemical and structural damage to proteins produced by synchrotron radiation, Proc. Natl Acad. Sci. U. S. A. 97 (2000) 623–628.
[79] I. Schlichting, J. Berendzen, K. Chu, A.M. Stock, S.A. Maves, D.E. Benson, R.M. Sweet, D. Ringe, G.A. Petsko, S.G. Sligar, The catalytic pathway of cytochrome P450cam at atomic resolution, Science 287 (2000) 1615–1622.
[80] G.I. Berglund, G.H. Carlsson, A.T. Smith, H. Szoke, A. Henriksen, J. Hajdu, The catalytic pathway of horseradish peroxidase at high resolution, Nature 417 (2002) 463–468.
[81] M. Wikström, Energy-dependent reversal of the cytochrome oxidase reaction, Proc. Natl Acad. Sci. USA 78 (1981) 4051–4054.
[82] L.C. Weng, G.M. Baker, Reaction of hydrogen peroxide with the rapid form of resting cytochrome oxidase, Biochemistry 30 (1991) 5727–5733.
[83] D.A. Proshlyakov, M.A. Pressler, G.T. Babcock, Dioxygen activation and bond cleavage by mixed-valence cytochrome *c* oxidase, Proc. Natl Acad. Sci. USA 95 (1998) 8020–8025.
[84] M. Fabian, W.W. Wong, R.B. Gennis, G. Palmer, Mass spectrometric determination of dioxygen bond splitting in the "peroxy" intermediate of cytochrome c oxidase, Proc. Natl Acad. Sci. USA 96 (1999) 13114–13117.
[85] W. Humphrey, A. Dalke, K. Schulten, VMD—visual molecular dynamics, J. Mol. Graph. 14 (1996) 33–38.
[86] L. Laaksonen, A graphics program for the analysis and display of molecular dynamics trajectories, J. Mol. Graph. 10 (1992) 33–34.